



**HAL**  
open science

## Identification of 7B04 aluminum alloy anisotropy yield criteria with conventional test and Pottier test at elevated temperature

Z. Wang, S. Zang, X. Chu, S. Zhang, Lionel Leotoing

► **To cite this version:**

Z. Wang, S. Zang, X. Chu, S. Zhang, Lionel Leotoing. Identification of 7B04 aluminum alloy anisotropy yield criteria with conventional test and Pottier test at elevated temperature. Results in Physics, 2019, 15, pp.102655. 10.1016/j.rinp.2019.102655 . hal-02310257

**HAL Id: hal-02310257**

**<https://univ-rennes.hal.science/hal-02310257>**

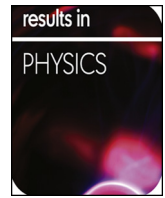
Submitted on 10 Jul 2020

**HAL** is a multi-disciplinary open access archive for the deposit and dissemination of scientific research documents, whether they are published or not. The documents may come from teaching and research institutions in France or abroad, or from public or private research centers.

L'archive ouverte pluridisciplinaire **HAL**, est destinée au dépôt et à la diffusion de documents scientifiques de niveau recherche, publiés ou non, émanant des établissements d'enseignement et de recherche français ou étrangers, des laboratoires publics ou privés.



Distributed under a Creative Commons Attribution - NonCommercial - NoDerivatives 4.0 International License



## Identification of 7B04 aluminum alloy anisotropy yield criteria with conventional test and Pottier test at elevated temperature

Zhihao Wang<sup>a</sup>, Shunlai Zang<sup>b</sup>, Xingrong Chu<sup>a,\*</sup>, Shunying Zhang<sup>c</sup>, Leotoing Lionel<sup>d</sup>

<sup>a</sup> School of Mechanical, Electrical and Information Engineering, Shandong University, Weihai 264209, China

<sup>b</sup> Key Laboratory of Education Ministry for Modern Design and Rotor-Bearing System, Xi'an Jiaotong University, No. 28 Xianning Road, Xi'an 710049, China

<sup>c</sup> Institute for Frontier Materials, Deakin University, Geelong Waurn Ponds, VIC 3220, Australia

<sup>d</sup> INSA-LGCGM-EA 3913, 20 Av. Des Buttesde Coësmes, CS70839, 35708 Rennes Cedex 7, France

### ARTICLE INFO

#### Keywords:

7B04 aluminum alloy  
Heterogeneous strain fields  
Yield criterion  
Inverse identification  
Deep drawing test

### ABSTRACT

7B04 aluminum alloy is widely used for strength critical aerospace structural applications. In this paper, the plastic anisotropy of this alloy at 200 °C was investigated based on Hill'48 and Yld2000-2D yield criteria. Thermal tensile test at setting temperature was carried out by a designed electrical heating system and the strain field was measured by the digital image correlation system simultaneously. Parameters of Hill'48 yield criterion with Voce hardening were determined directly based on the thermal tensile test. The parameters of Yld2000-2D criterion were obtained by the inverse identification method with Pottier test at elevated temperature which can generate heterogeneous strain fields. Deep drawing test was carried out at 200 °C and the earing heights were measured. The accuracy of the determined yield criteria parameters was validated by numerical and experimental deep drawing test results.

### Introduction

7B04 aluminum alloy is a high-strength alloy which is widely used in the aerospace industry because of high intensity, corrosion resistance and good toughness [1,2]. Due to heat treatment and rolling process, there is anisotropic behavior with a certain degree for 7B04 aluminum alloy sheet. This property has a significant influence on the quality of the sheet metal forming. Now, finite element method (FEM) is widely used in the prediction of the sheet metal forming. An accurate anisotropic yield criterion can lead to a good prediction of the metal sheet plastic behavior, e.g. [3,4]. In order to obtain the optimized forming process, accurate constitutive model is required. And the accurate description of plastic anisotropy is a key point.

Many anisotropic yield criteria were developed to characterize the plastic anisotropy of metals. Under plane stress condition, Hill'48 [5] yield criterion includes four parameters which can be obtained by conventional uniaxial tensile tests. With the development of anisotropic yield criteria, they tend to become more advanced involving more parameters, such as Yld2000-2D [6] and Bron & Besson [7]. Although advanced yield criteria can more accurately describe the material plastic anisotropy, they require more multi-axial stress states experimental data to identify parameters. However, a kind of conventional test only provided one stress state experimental data. Thus, the

parameters identification process is heavy in workload and complex in calculation. And for this reason, the usage of the advanced yield criteria is usually limited. In addition, traditional standard tests which limit the identification of the yield criteria parameters to homogeneous strain state may lead to an incomplete characterization of plastic anisotropy in the complex forming of metal sheets [8].

In view of the shortcomings of the traditional standard test in determining the advanced yield criteria parameters, many complex geometries specimens were designed for non-standard tests. These specially designed specimens usually with varying cross-section or including holes. Compared with conventional test specimen, non-standard specimen can show more obvious heterogeneous strain state in tests. From heterogeneous strain fields, more information can be obtained. Therefore, yield criteria parameters obtained by heterogeneous strain fields can more accurately predict the plastic behavior of metals under complex strain paths [9]. In addition, if the specimen of non-standard test was well designed, constitutive parameters can be identified simultaneously from a single test [10]. Thus, non-standard test reduced the number of tests as well as avoiding the limitation of the plastic anisotropy characterization by the homogeneous deformation. Since the DIC (Digital Image Correlation) technology has been developed, heterogeneous strain fields in non-standard specimens can be easily obtained. This has led to the development of new tests and methods for

\* Corresponding author.

E-mail address: [xrchu@sdu.edu.cn](mailto:xrchu@sdu.edu.cn) (X. Chu).

<https://doi.org/10.1016/j.rinp.2019.102655>

Received 14 August 2019; Received in revised form 10 September 2019; Accepted 10 September 2019

Available online 13 September 2019

2211-3797/ © 2019 The Authors. Published by Elsevier B.V. This is an open access article under the CC BY-NC-ND license (<http://creativecommons.org/licenses/by-nc-nd/4.0/>).

identification of the constitutive equation parameters. However, due to the heterogeneous strain field obtained by the non-standard test has no directly analytical relationship with the constitutive equation parameters, parameters cannot be directly obtained from these non-standard tests. Therefore, an inverse identification method is required.

Many researchers have summarized the identification methods for the material constitutive models [11–13]. As summarized by those papers, kinds of identification methods based on full-field measurements have been developed to obtain the constitutive equation parameters, namely the finite element model updating method (FEMU), the constitutive equation gap method (CEGM), the virtual fields method (VFM), the equilibrium gap method (EGM) and the reciprocity gap method (RGM). FEMU method is a very widespread approach for parameters identification, e.g. [14–16]. It determined the constitutive equation parameters by updating the parameter set in the finite element model to achieve the best match with the experimental results. In this paper, the FEMU method was chosen.

Recently, some works have focused on parameter identification of yield criteria from the non-standard tests. Souto et al. [17] presented a new optimization method for designing heterogeneous tests. Based on the Nelder-Mead algorithm, the geometry of the specimen can be automatically optimized in the ABAQUS for the purpose of maximizing the strain state of the specimen. Zhang et al. [18] designed a biaxial tensile specimen with notches which can simultaneously obtain different strain paths. Based on the inverse identification method, the parameters of the Bron and Besson yield criterion were identified with only one test. Zhu et al. [19] used the plane strain test to replace the equi-biaxial tensile test. Combined with the Simplified method, the parameters of Yld2000-2D yield function for 5xxx aluminum alloy and AlMgSi alloy sheets were accurately identified. Teaca et al. [20] identified the Makkouk and Morreale (FMM) yield criterion parameters by non-standard biaxial tensile tests. Two types of cruciform specimens with holes can generate heterogeneous strain fields. Based on minimizing the gap between experimental and simulated strain fields, parameters were accurately obtained. In order to guarantee strain heterogeneity and exhibit strain paths from uniaxial to equi-biaxial tension, Prates et al. [21] designed a non-standard cruciform specimen. Parameters of Hill'48 yield criterion with Swift hardening law were identified by methodology of simulation-experiment combination. Pottier et al. [22] used three shapes of tensile specimens to investigate the effects of heterogeneous strain fields on the result of inverse identification. The first specimen was a standard tensile specimen, the second one with a hole and the third one was a shear-like tensile specimen. Combined with DIC technology and FEMU method, the study found that the ability of predicting the real deformation process was improved when the strain heterogeneity increased. Kim et al. [10] designed several types of uniaxial tensile specimens which provided heterogeneous strain fields. And the VFM method was adopted to determine the parameters of Hill'48 model with Swift hardening. Rossi M et al. [23] designed a notched specimen to produce a rather heterogeneous strain field. Based on the VFM method and the notched specimen, the authors identified the parameters of Yld2000-2D. Denys et al. [24] designed a double perforated specimen which can generate complex displacement fields. With a multi-DIC setup, displacement fields on multiple surfaces of the specimen were measured. Based on the obtained displacement fields, the Hill'48 parameters were identified by the FEUM method. Pottier et al. [25] designed a specimen with the heterogeneous strain fields which can exhibit tensile, shear and expansion strain states. Based on the FEMU method and designed specimen, Hill'48 yield criterion was determined and validated by the deep drawing test. The result showed that identification based on heterogeneous tests presented better precision.

In this paper, an electric heating system was designed for the thermal uniaxial tensile test, and a heated Pottier test with FEMU method was used for the anisotropy yield criterion identification. In order to demonstrate the utility of the electric heating system and the

heated Pottier test with FEMU method, the plastic anisotropy identification tests of 7B04 aluminum alloy were carried out at 200 °C. The Hill'48 determined by the uniaxial tensile tests with electrical heating system and Yld2000-2D yield criteria determined by the Pottier test were adopted for the material anisotropy behaviour characterization. Finally, the earing heights of deep drawing test were measured, and the validation of the identification methods and heating methods was discussed.

## Material model

### Hill'48 yield criterion

Hill'48 yield criterion is widely used to describe the anisotropy of aluminum alloy sheet. With plane stress condition ( $\sigma_{13} = \sigma_{23} = \sigma_{33} = 0$ ), it can be written as:

$$\bar{\sigma}^2 = (G + H)\sigma_{11}^2 + (H + F)\sigma_{22}^2 - 2H\sigma_{11}\sigma_{22} + 2N\sigma_{12}^2 \quad (1)$$

where  $\sigma_{ij}$  are the Cauchy stress tensor components,  $\bar{\sigma}$  is the equivalent stress.  $F$ ,  $G$ ,  $H$  and  $N$  are yield criterion parameters. Those parameters can be calculated from three plastic strain ratio ( $r$ -value)  $r_0$ ,  $r_{45}$  and  $r_{90}$ . The  $r$ -value is defined by:

$$r = \frac{\varepsilon_b}{\varepsilon_a} \quad (2)$$

where  $\varepsilon_b$  is the true plastic thickness strain,  $\varepsilon_a$  is the true plastic width strain. The parameters  $F$ ,  $G$ ,  $H$  and  $N$  can be calculated by:

$$F = \frac{r_0}{(1+r_0)r_{90}}G = \frac{1}{(1+r_0)}H = \frac{r_0}{(1+r_0)}N = \frac{(1+2r_{45})(r_0+r_{90})}{2(1+r_0)r_{90}} \quad (3)$$

### Yld2000-2D yield criterion

Yld2000-2D yield criterion with eight anisotropy coefficients was proposed by Barlat et al. [6]. It can more accurately describe the anisotropic behaviour of aluminum alloy sheets. The function is given by:

$$\Phi' + \Phi'' = 2\sigma^m \quad (4)$$

$$\Phi' = |X'_1 - X'_2|^m \quad (5)$$

$$\Phi'' = |2X''_2 + X''_1|^m + |2X''_1 + X''_2|^m \quad (6)$$

$$X'_i = \frac{1}{2}(X'_{11} + X'_{22} \pm \sqrt{(X'_{11} - X'_{22})^2 + 4X'^2_{12}}) \quad (7)$$

$$X''_j = \frac{1}{2}(X''_{11} + X''_{22} \pm \sqrt{(X''_{11} - X''_{22})^2 + 4X''^2_{12}}) \quad (8)$$

$$\mathbf{X}' = \mathbf{L}'\boldsymbol{\sigma}\mathbf{X}' = \mathbf{L}'\boldsymbol{\sigma} \quad (9)$$

where  $X'_i$  and  $X''_j$  are the principle values of the matrices  $X'$  and  $X''$ .  $\boldsymbol{\sigma}$  is Cauchy stress and the  $L'$  and  $L''$  are expressed as:

$$\begin{bmatrix} L'_{11} \\ L'_{12} \\ L'_{21} \\ L'_{22} \\ L'_{66} \end{bmatrix} = \begin{bmatrix} 2/3 & 0 & 0 \\ -1/3 & 0 & 0 \\ 0 & -1/3 & 0 \\ 0 & 2/3 & 0 \\ 0 & 0 & 1 \end{bmatrix} \begin{bmatrix} \alpha_1 \\ \alpha_2 \\ \alpha_7 \end{bmatrix} \quad (10)$$

$$\begin{bmatrix} L''_{11} \\ L''_{12} \\ L''_{21} \\ L''_{22} \\ L''_{66} \end{bmatrix} = \frac{1}{9} \begin{bmatrix} -2 & 2 & 8 & -2 & 0 \\ 1 & -4 & -4 & 4 & 0 \\ 4 & -4 & -4 & 1 & 0 \\ -2 & 8 & 2 & -2 & 0 \\ 0 & 0 & 0 & 0 & 9 \end{bmatrix} \begin{bmatrix} \alpha_3 \\ \alpha_4 \\ \alpha_5 \\ \alpha_6 \\ \alpha_8 \end{bmatrix} \quad (11)$$

In the above equations,  $\alpha_1$ – $\alpha_8$  are eight anisotropy coefficients. In this work  $m = 8$ , since 7B04 aluminum alloy is an FCC material.

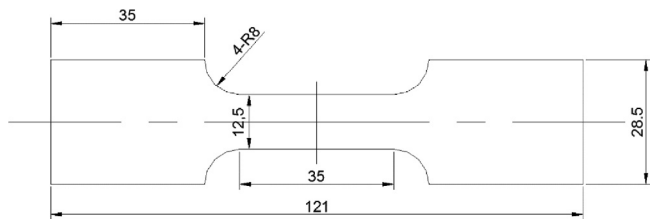


Fig. 1. Geometry and dimensions of tensile test specimen (in mm).

### Voce hardening rule

Hardening behavior was described using the Voce hardening rule:

$$\bar{\sigma} = A + K(1 - e^{-n \cdot \varepsilon_p^{eq}}) \quad (12)$$

where  $\bar{\sigma}$  is the equivalent stress,  $\varepsilon_p^{eq}$  is the equivalent plastic strain.  $A$ ,  $K$ ,  $n$  are fitting parameters.

### Experiments

#### Uniaxial tensile test

The material used in this paper was 7B04 aluminum alloy with nominal thickness of 2.0 mm. The tensile specimens were cut at 0° (RD), 45° and 90° (TD) from the rolling direction of the sheet using laser-cut. Fig. 1 illustrates the geometry of the specimen. In order to investigate plastic anisotropy property, the tensile test was conducted under displacement control in a mechanical universal testing machine at a tensile speed of 2.1 mm/min, corresponding to a strain rate of  $0.001 \text{ s}^{-1}$ . Specimen temperature during the test was controlled at 200 °C by an electrical heating system (Fig. 2). Through electrical resistance heating method, specimen was heated when low-voltage high-current direct current (DC) flowed through. At the same time, temperature was monitored by a thermocouple wire welded in the center of the specimen. The thermocouple wire transmitted the signal to PLC controller, and the value of DC can be regulated under the feedback adjustment. It ensured that the temperature of specimen was stable at the target value, and the temperature fluctuation under the PLC controller was below 3 °C. Electrical heating system can avoid the limitation of DIC technology in the traditional heating furnace, and its heating was more efficient. In the DC-assisted uniaxial tensile test, the thermal effect generated by DC has a much higher impact on plastic behaviour of sheet metal than the athermal effect [26–29]. In this work, the DC density is below  $8 \text{ A/mm}^2$ , thus only thermal effect was considered with specimens heated to 200 °C.

In the electric heating process, the fixture of tensile test machine can

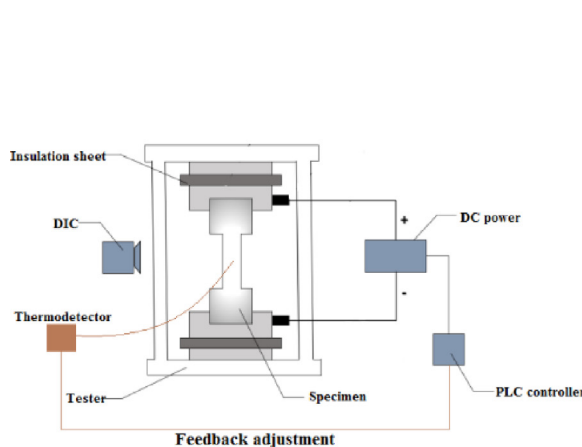


Fig. 2. Schematic diagram and picture of the electrical heating system.

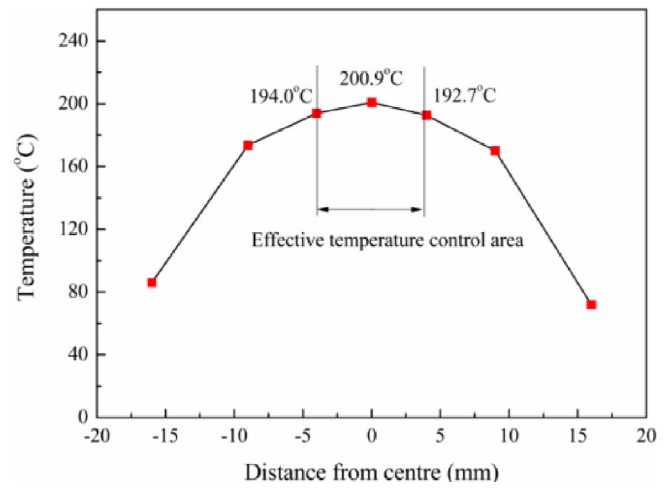


Fig. 3. Multi-point temperature measurement results along the centerline of specimen.

affect the temperature distribution of the test specimen. The temperature distribution along the longitudinal direction of the specimen was obtained by 7 thermocouples. Through multi-point temperature measurement results (Fig. 3), it was found that the temperature in the central area of the specimen was the highest, while the temperature was lower near the fixture. Temperature difference in the effective temperature control area was presented in Fig. 3. It was shown that the temperature variation was less than 8 °C at 200 °C. Although there are some temperature differences in the effective temperature control area, its influence for the uniaxial tensile test was acceptable [30]. The center area with high temperature (200 °C) was easier to deform, this causes the necking to occur at the specimen center. And the force recorded by the tensile test machine reflects the mechanical properties of the high temperature specimen area. In order to obtain accurate mechanical properties of the specimen at 200 °C, a strain measurement area (Fig. 4) within the effective temperature control area was selected to obtain the strain field with DIC system. Two high resolution CCD cameras ( $1624 \times 1236$  pixels) were used to capture the pictures and the photo-frequency was set to 4 images/s. In this work, to determine the strain and displacement fields distribution, the subset size of 10 pixels and the step size of 10 pixels were set in the DIC system.

The true stress-strain curves measured along three different directions were plotted in Fig. 5. From this picture, anisotropy can be observed. The hardening behavior of 7B04 aluminum alloy was fitted by Voce hardening, and the fitted formulas were shown in Fig. 5. Table 1 presented the basic mechanical properties of 7B04 aluminum alloy. It

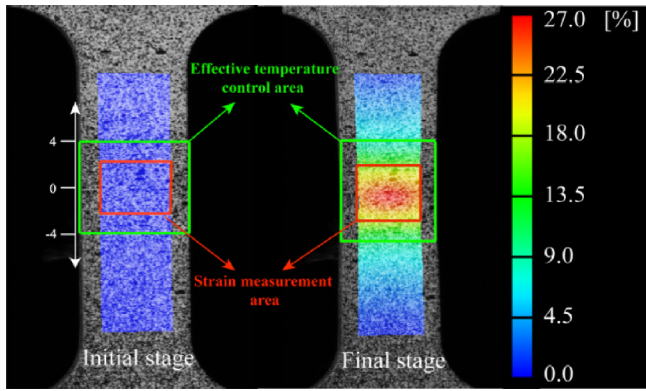


Fig. 4. Selected strain measurement area within the effective temperature control area.

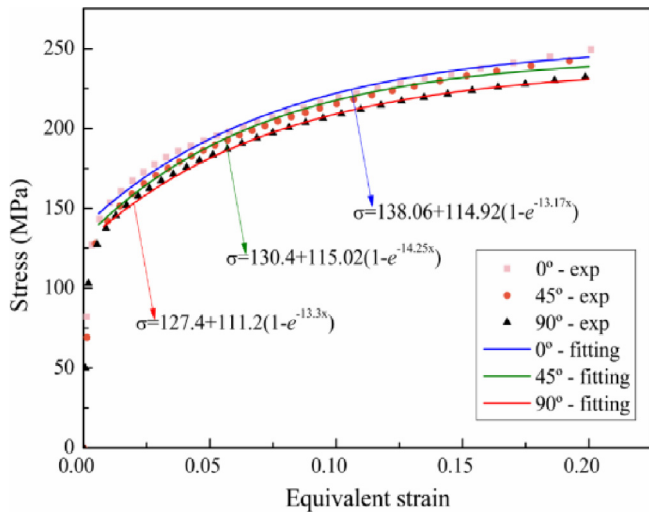


Fig. 5. True stress-strain curves of 7B04 aluminum alloy.

Table 1  
Basic mechanical properties of 7B04 aluminum alloy.

Material	E (MPa)	$\mu$	$\sigma_0$ (MPa)	$\sigma_{45}$ (MPa)	$\sigma_{90}$ (MPa)
7B04	60471.07	0.325	138.06	130.4	127.4

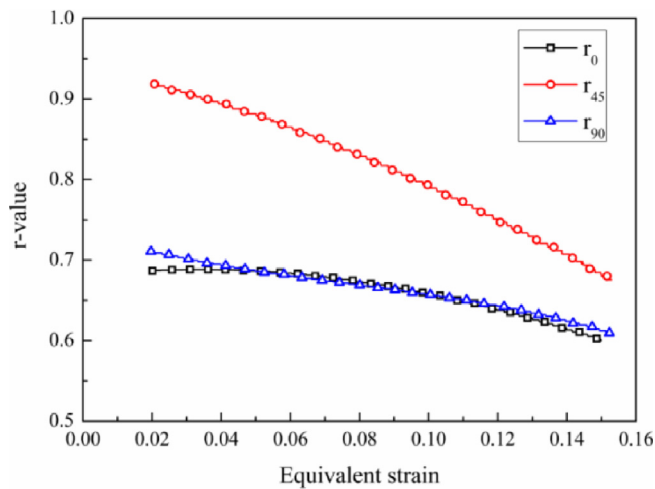


Fig. 6. Evolution of  $r$ -value in the  $\bar{\epsilon}$  range [0.02, 0.15] along three directions.

Table 2  
 $r$ -value calculated different plastic strain ranges.

$\bar{\epsilon}$	$r_0$	$r_{45}$	$r_{90}$
0.02–0.1	0.685	0.864	0.676
0.1–0.15	0.633	0.739	0.648
0.02–0.15 (selected)	0.671	0.816	0.667

Table 3  
Calculated Hill'48 parameters.

F	G	H	N
0.602	0.598	0.402	1.579

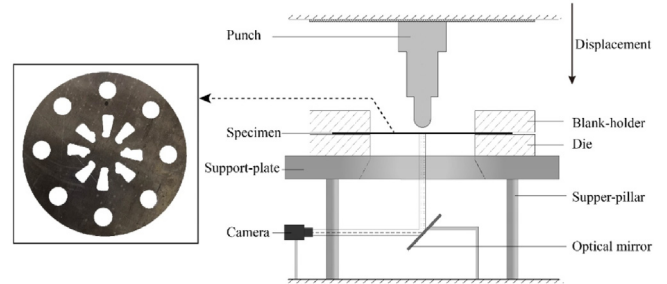


Fig. 7. Specimen picture and device schematic diagram of the Pottier test.

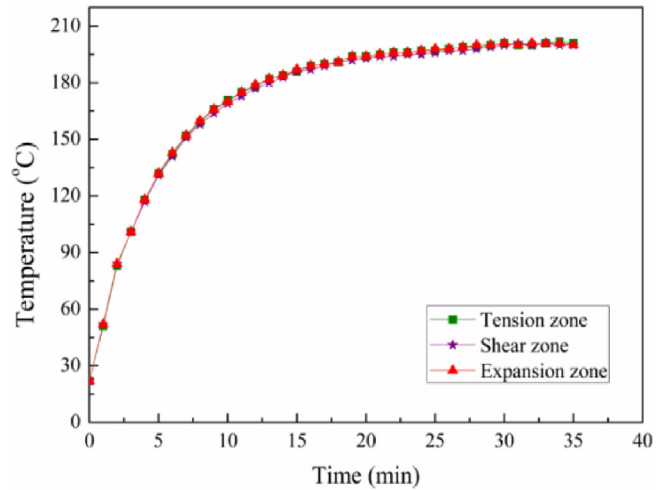


Fig. 8. Heating results of Pottier specimen.

was well known that when the necking occurred, the stress field became a heterogeneous field. If not corrected, the stress-strain curve after necking had no guiding significance for material application. Therefore, only data before necking was adopted in this work.

Plastic strain ratio ( $r$ -value) is an important index for anisotropy characterization, and it varied with the plastic deformation. Fig. 6 showed the evolution of  $r$ -value in the  $\bar{\epsilon}$  range [0.02, 0.15] along three directions. For 7B04 aluminum alloy, the  $r$ -value curve of 45° direction was clearly higher than the other two directions, and curves of the RD and TD were similar. The  $r$ -values gradually decreased with the increasing deformation. In order to obtain the Hill'48 anisotropy parameters, an average value of  $r$ -value was used in this study, which was listed in Table 2. And the parameters of Hill'48 yield criterion were listed in Table 3.

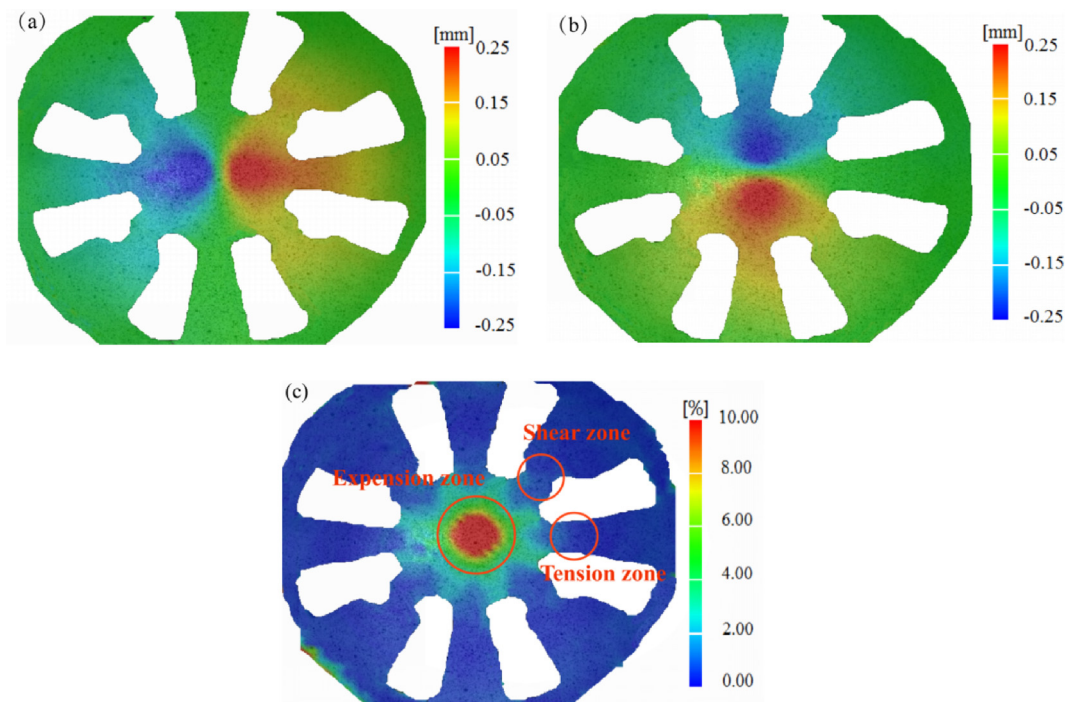


Fig. 9. Displacement and strain fields of Pottier specimen (punch stroke 4 mm). (a)  $u_x$  displacement field (b)  $u_y$  displacement field (c) Strain field.

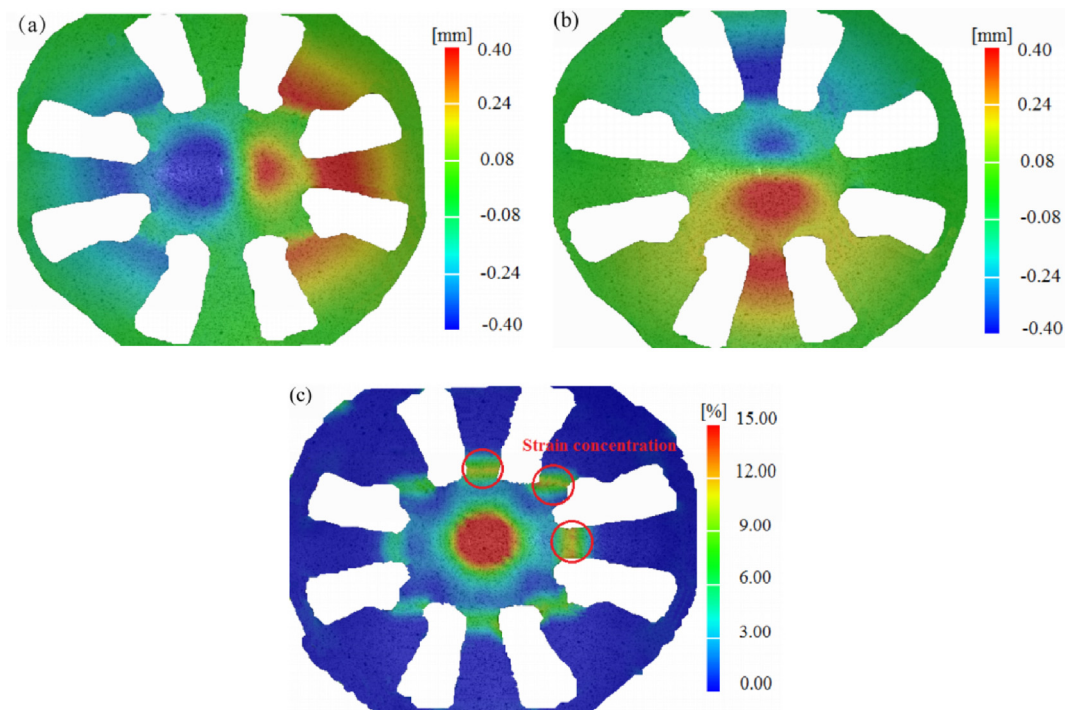


Fig. 10. Displacement and strain fields of Pottier specimen (punch stroke 8.33 mm). (a)  $u_x$  displacement field (b)  $u_y$  displacement field (c) Strain field.

*Pottier specimen test*

The Pottier test was in order to offer information for the constitutive parameter inverse identification, and the adopted specimen was designed by Pottier [25]. Specimens were manufactured by laser-cut from 7B04 aluminum alloy sheet. As illustrated in Fig. 7, diameter and thickness of the Pottier specimen was 130 mm and 2.0 mm, respectively. This specimen was designed to increase the strain heterogeneous as well as exhibiting tension, shear and expansion behaviors. Multi-

angle tension and shear zones along the rolling direction can fully show the anisotropy of the test material. A hemispherical hollow punch (diameter  $\varnothing 15$  mm) was used to apply the prescribed displacement at the specimen center. The punch was connected with the mechanical universal testing machine by an upper template, the die and blank holder were mounted on a support plate. Specimen was fixed between die and blank holder by bolts to prevent the sliding between the specimen and the die or the blank holder, as shown in Fig. 7. Furthermore, the displacement speed of the punch was set to 1.667 mm/min

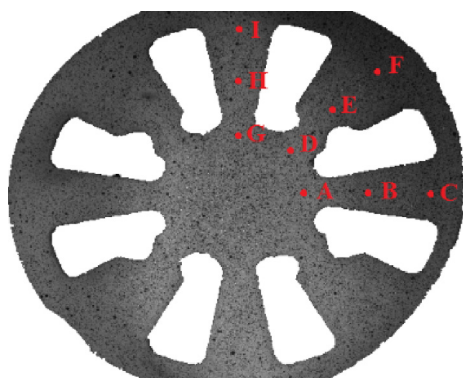


Fig. 11. Reference points used for inverse identification.

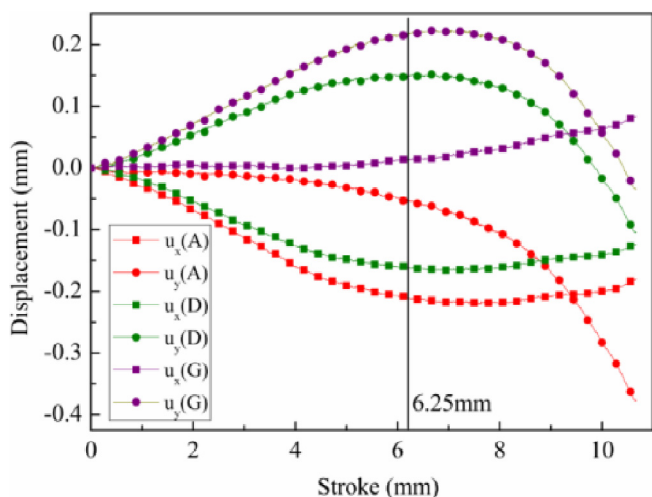


Fig. 12. Displacement curves of reference points (A, D, G) within the expansion zone.

according to the strain rate of tensile test.

During the deformation, displacement field on the specimen surface was measured with the DIC. With two cameras, DIC can accurately measure the out-of-plane displacement. Prior to the testing, specimens were painted with a random speckle pattern over an undercoat of white paint. Then the deformation of the speckle pattern was captured using a digital camera with an acquisition rate of 4 image/s. Finally, based on those digital images, displacement fields were calculated by post-processing with DIC software. For the convenience of taking photos from a horizontal direction, an optical flat mirror was placed at 45 degrees below the die.

In this work, in order to carry out the Pottier test at 200 °C, a heating rod was installed in the hollow of the punch, and sixteen heating rods

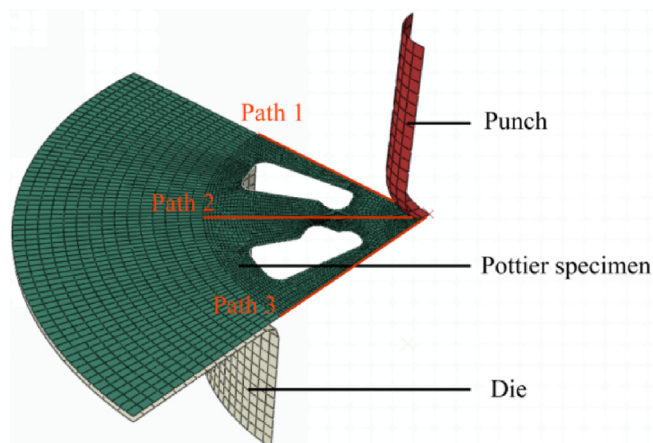


Fig. 14. Analysis section and visualization of 3 paths and FE model of Pottier test.

were installed in the hollows along the circumference of the die and the blank holder. The temperature of heating rods was controlled by two PID-controllers, respectively. And the heating result of the Pottier specimen was presented in Fig. 8. After 30 min of heating, the temperatures of each part of the specimen were stably maintained at 200 °C. Then the punch started to push down.

When the stroke was 4 mm, the experimental measurement of displacement ( $u_x, u_y$ ) fields was presented in Fig. 9(a) and (b). In the early stages of deformation, the displacement fields were nearly symmetrically distributed because of the geometrical symmetry of the Pottier specimen. As can be seen from Fig. 9(c), the expansion zone was the main deformation area. When the stroke was 8.33 mm, the strain concentration appeared on the upper right side of the specimen in Fig. 10(c), tension and shear zones were necked. With the punch pushing down, the main deformation zones moved from the expansion zone to the shear and tension zones.

Considering this phenomenon, the upper right side of the specimen was selected as the inverse identification displacement reference area. For the accuracy of parameters inverse identification, nine reference points were selected, as shown in Fig. 11. The displacement curves of reference points showed that points within the expansion area have a phenomenon of inverse displacement, which was caused by the movement of the main deformation zone, as shown in Fig. 12. In addition, for the Pottier specimen, it was difficult to reproduce the necking phenomenon with only one corner in the finite element simulation. Therefore, in order to enhance the inverse identification result accuracy, the displacement data before the stroke of 6.25 mm were used. Analysis of the specimen strain field under this punch stroke showed that strain concentration began to occur in the tensile and shear zones, as can be seen in Fig. 13(a). And the strain states (Fig. 13(b)) showed that the Pottier specimen generated very heterogeneous strain

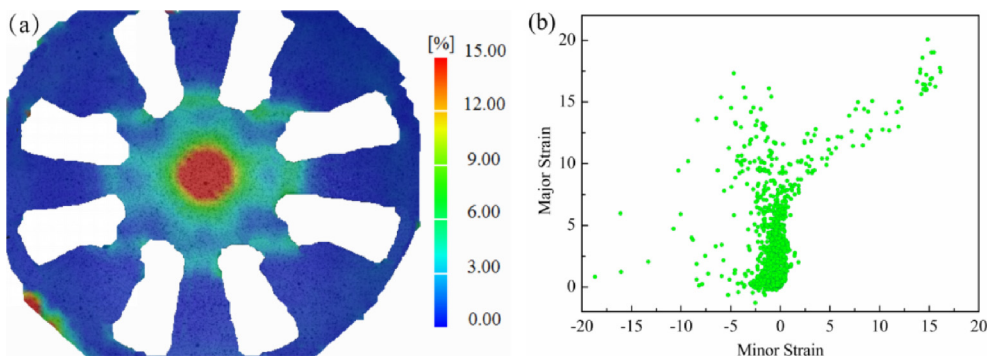


Fig. 13. Strain field and states of Pottier specimen when the stroke was 6.25 mm (a) Strain field (b) Strain states.

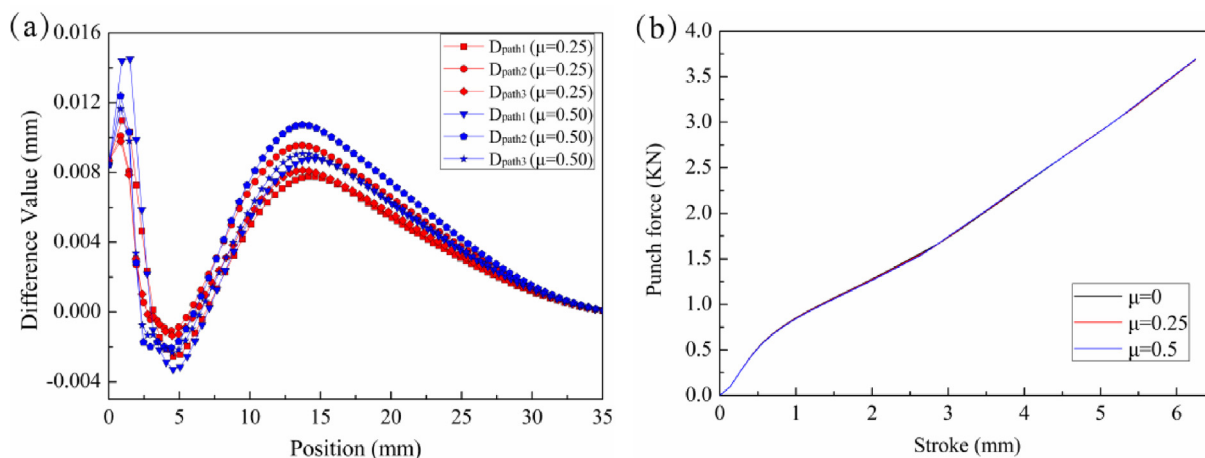


Fig. 15. Simulated results with different friction coefficients along different paths (a) Displacement difference value (b) Punch force curves.

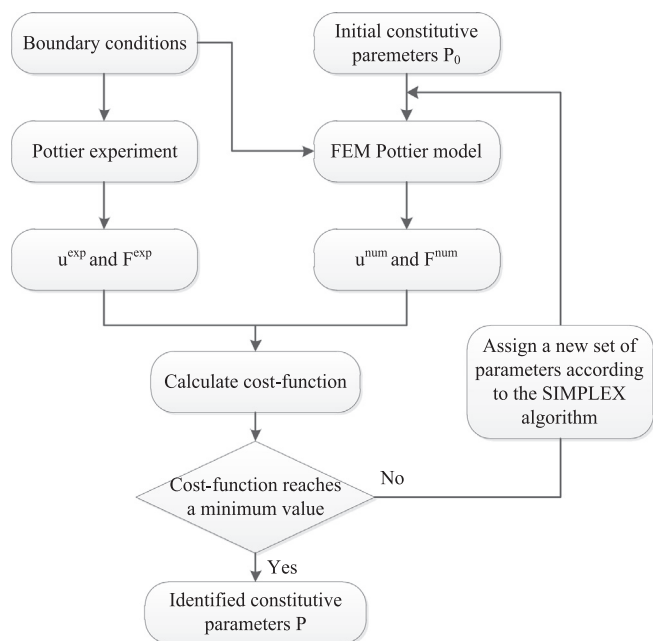


Fig. 16. Flowchart of inverse identification process for constitutive equation parameters.

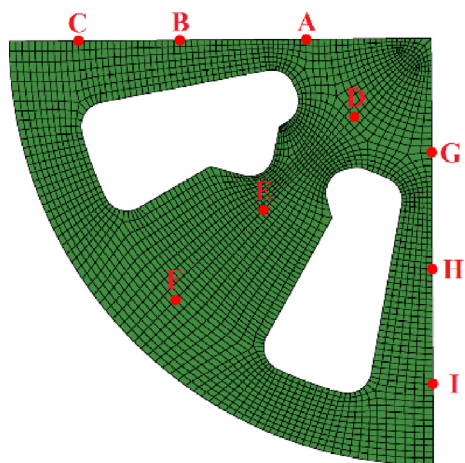


Fig. 17. Reference points in FE-Pottier model used for displacement output.

Table 4  
Identified parameters of Yld2000-2D yield criterion.

Parameters	$\alpha_1$	$\alpha_2$	$\alpha_3$	$\alpha_4$	$\alpha_5$	$\alpha_6$	$\alpha_7$	$\alpha_8$
Initial values	1	1	1	1	1	1	1	1
Identified values	0.955	0.991	0.923	1.092	1.091	0.902	0.901	0.984

fields, which included biaxial tensile strain state, plane strain state, uniaxial tensile strain state and shear strain state.

Finite element modeling of Pottier test

The Pottier test was accurately modeled according to the experiment conditions by using ABAQUS/Standard FE code. The FE-Pottier model consisted in three parts: a rigid hemispherical punch, a rigid die and a deformable specimen, as shown in Fig. 14. Due to symmetry, only one quarter of the model was modeled for the purpose of time saving. To describe the material elastic property, a Young’s modulus of 60471.07 MPa and a Poisson’s ratio of 0.325 were considered. The Yld2000-2D yield function with Voce hardening rule was implemented with a user subroutine UMAT. Specimen was meshed by the 4-node shell (S4) elements. In order to improve the accuracy of simulations, mesh refinement was performed in the main deformed areas of the specimen. A final element size of 0.2 mm in the main deformed areas was adopted. Prescribed displacement was imposed according to the test displacement at the punch with a speed of 1.667 mm/min. The non-deformed area of specimen and the die were remained immobile.

In order to determine the friction coefficient between the punch and specimen, the influence of friction on simulated punch force and displacement field were studied. The friction coefficient  $\mu$  was set to 0, 0.25 and 0.5 in three FE-Pottier models, respectively, and the displacement result of FE-Pottier model ( $\mu = 0$ ) was used as the reference value  $R_D$ . The displacement value obtained by the other friction coefficient models minus the reference value  $R_D$  was set as the displacement difference value. In addition, three different paths (Length = 35 mm) were selected to be the comparison paths, as shown in Fig. 14. The evolution of displacement difference value along three comparison paths were presented in Fig. 15(a). It was observed that the maximum displacement difference value ( $D_{path}$ ) was only 0.014 mm. Furthermore, the simulated punch force curves obtained under different friction coefficients were the same, as shown in Fig. 15(b). Therefore, considering that the friction coefficient has little effect on the accuracy of the simulated result, the friction coefficient was set to 0.25 in the inverse identification process in agreement with the former results [25].

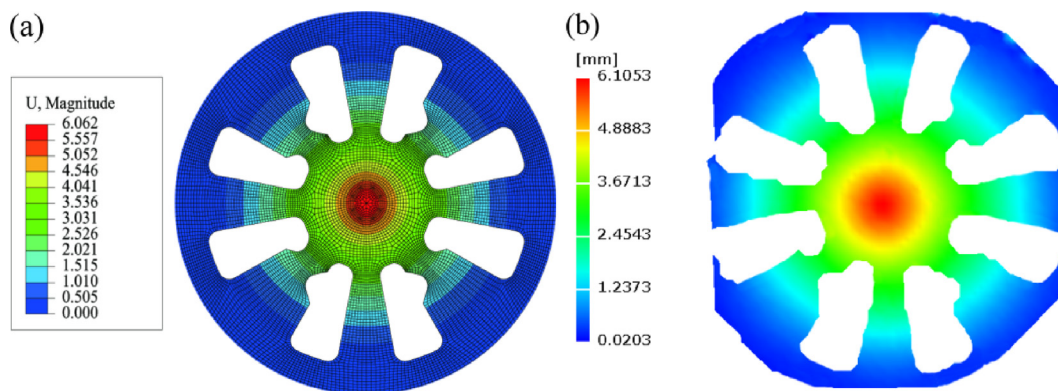


Fig. 18. (a) Simulation displacement field obtained by identified parameters (b) Experimental measured displacement field.

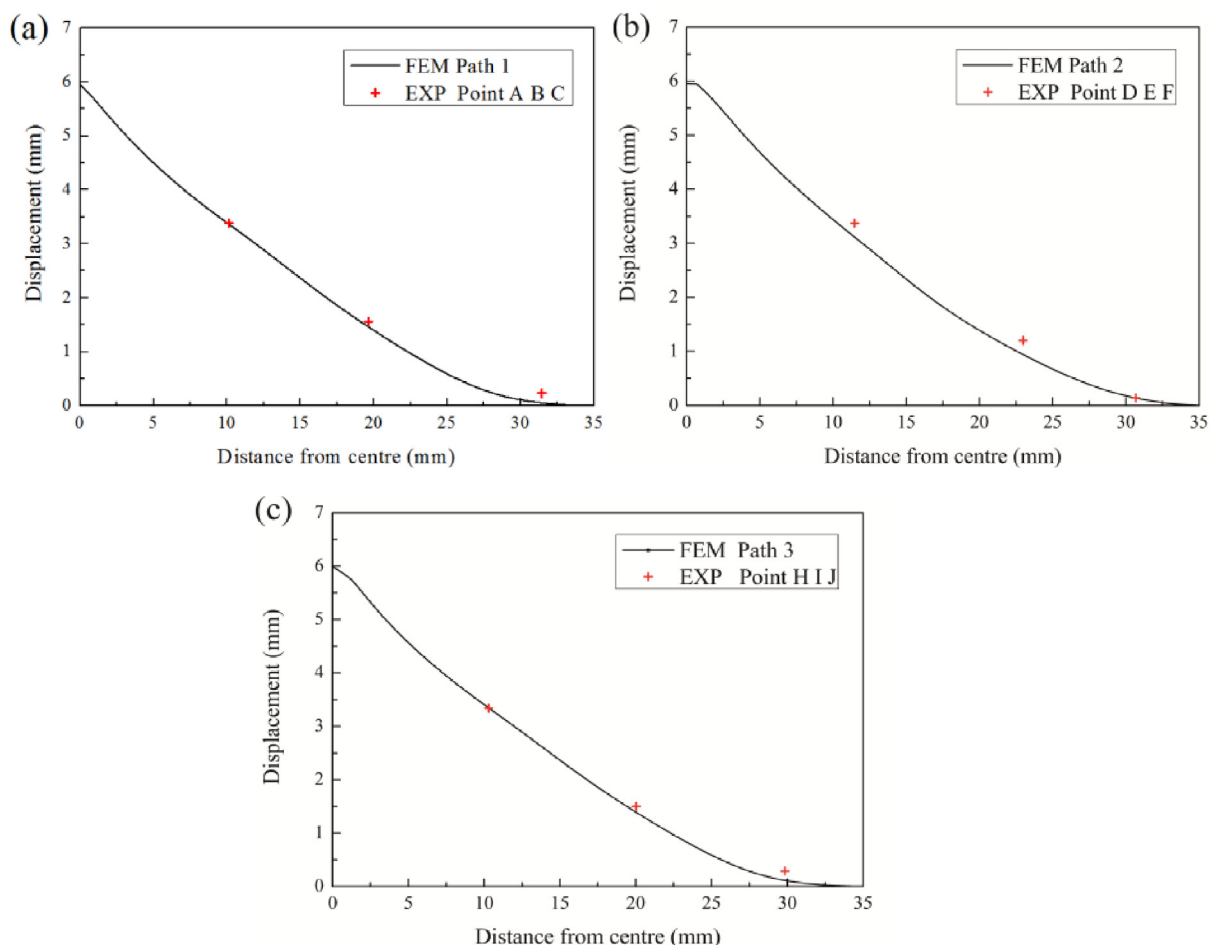


Fig. 19. Gaps between the simulation and experimental displacements of reference points. (a) Path 1 (b) Path 2 (c) Path 3.

**Inverse identification**

*Principle and flowchart*

The experimental data used for the constitutive equation parameters inverse identification included the displacement and punch force obtained by the Pottier test. Constitutive equation parameters were set in the FE-Pottier model, and a cost-function was used to calculate the gap between the experiment and simulation. Through updating the constitutive parameter sets in the FE-Pottier model, the FEMU method minimized the gap between the simulation and experimental results. As well known, the displacement field and forming force were sensitive to

the material yield function and hardening rule. Furthermore, the FEMU method based on the experimental data of displacements and force (FEMU-U-F) was better suited to problems involving stress and strain concentration [11]. Therefore, the FEMU-U-F method was adopted to obtain the constitutive equation parameters. The identification process was realized by the software mode-FRONTIER coupled with ABAQUS and MATLAB, and the process flowchart was shown in Fig. 16.

*Cost-function*

For the convenience of calculating the gap between the experimental and numerical results, nine reference points in FE-Pottier model

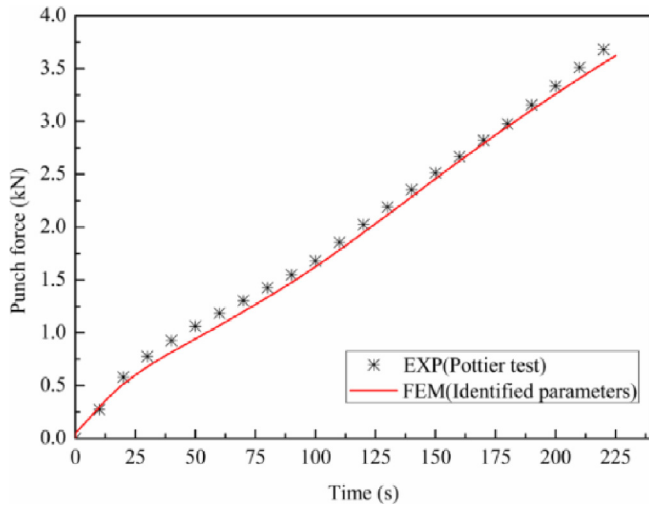


Fig. 20. Comparison of punch force between the simulation and experimental results.

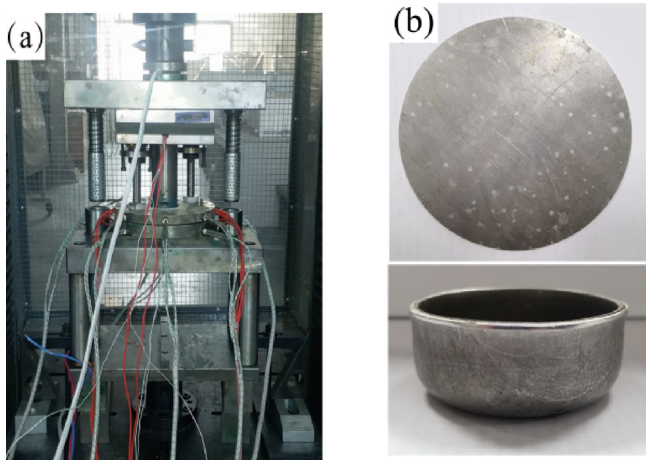


Fig. 21. (a) Deep drawing test device (b) Deep drawing test specimen.

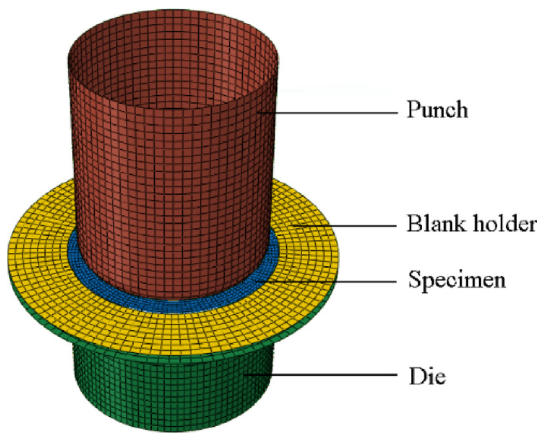


Fig. 22. FE model of deep drawing test.

corresponding to the positions in experiment were set, as shown in Fig. 17.

Displacement of the simulation reference points were compared to the experimental counterparts as well as the punch force, and the gap can be quantified with a weighted cost-function. Based on the selected FEMU-U-F method, the cost-function was consisted of force and displacement data as follows:

$$\begin{aligned}
 f(p) &= \frac{1}{2} \left[ \sum_{i,j=1}^{N_i, N_j} \left[ \left( \frac{u_x^{\text{exp}} - u_x^{\text{num}}}{\max(u_x^{\text{exp}})} \right) + \left( \frac{u_y^{\text{exp}} - u_y^{\text{num}}}{\max(u_y^{\text{exp}})} \right) + \left( \frac{u_z^{\text{exp}} - u_z^{\text{num}}}{\max(u_z^{\text{exp}})} \right) \right. \right. \\
 &\quad \left. \left. + 9 \left( \frac{F^{\text{exp}} - F^{\text{num}}}{\max(F^{\text{exp}})} \right) \right] \right] \quad (13)
 \end{aligned}$$

where  $p$  represented a set of parameters,  $u^{\text{exp}}$  and  $u^{\text{num}}$  were DIC-measured and FEM-calculated displacements, respectively.  $u_x$ ,  $u_y$ ,  $u_z$  were the displacements along the  $x$ ,  $y$ ,  $z$  axis, respectively.  $F$  was the punch force.  $N_i$  was the number of reference points and  $N_j$  was the number of considered time steps. In this paper,  $N_j$  equaled to 45 (every 5 s as a time step, and the effective test time was 225 s). In order to balance the weight between the displacement and force, a weight coefficient of 9 was used in the cost-function.

### Optimization algorithm

Various optimization algorithms were proposed to solve non-linear objective optimization problems. In this paper, the SIMPLEX algorithm was preferred in the identification process. The SIMPLEX optimization algorithm implemented in mode-FRONTIER was used for finding the minimum of an objective function in a multi-parameters problem. It was initialized with  $N + 1$  sets of constitutive equation parameters combinations ( $N$  was the number of input constitutive equation parameters). Firstly, it constructed a polyhedron with  $N + 1$  vertices and compared the values of the objective function at  $N + 1$  vertices. Then, it moved the polyhedron towards the optimal point by iteratively replacing the worst vertex with a sequence of geometric transformations [31]. The  $N + 1$  sets of initial constitutive equation parameters were randomly selected within the variation ranges of the parameters.

The initial values of parameters were set to 1, and the value ranges were between 0.5 and 1.5. After 500 steps of the updating process and evaluation, 8 parameters of the constitutive model were simultaneously identified. The result was shown in Table 4. The displacement fields obtained by simulation with the identified parameters and experimental measurement were shown in Fig. 18. The gaps between the simulation and experimental displacements of reference points were presented in Fig. 19. The gaps between the simulation and experimental punch force were shown in Fig. 20. Although it existed some gaps, the FEMU-U-F method led to an available fit between the experimental and simulation results. These gaps were caused by constitutive model parameters approximation, measuring error and FE modeling.

### Validation: deep drawing test

A deep drawing test at 200 °C was carried out for the purpose of checking the accuracy of the constitutive equation parameters. The deep drawing device was shown in Fig. 21(a). Heating method was the same as the Pottier test. Displacement speed of the punch was set to 2.667 mm/min according to the strain rate of tensile test. The circular specimen with a diameter of 80 mm and a thickness of 2 mm was cut from 7B04 aluminum alloy sheet by using laser-cut. During the test, the stable blank holder force (6 kN) was realized by two nitrogen springs. The upper profile of the deep drawn cup (Fig. 21(b)) was measured by a height gauge, and the earing height exhibited the material anisotropy.

As shown in Fig. 22, the FE model was used to simulate the deep drawing test. The punch, die and blank holder were modeled by the discrete rigid bodies, while the specimen was modeled by the deformable shell. The friction coefficient between the punch and specimen was set to 0.25 in agreement with the FE-Pottier model. Prescribed displacement was imposed according to the test displacement at the punch, and the die remains fixed. In addition, a 6 kN force was directly applied on the blank-holder. The constitutive parameter sets obtained by conventional uniaxial tensile and inverse identification method were

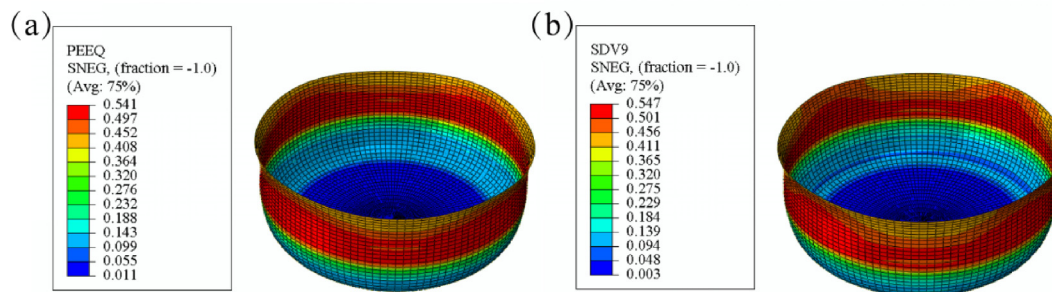


Fig. 23. Simulation equivalent plastic strain field by (a) Hill'48 (b) Yld2000-2D.

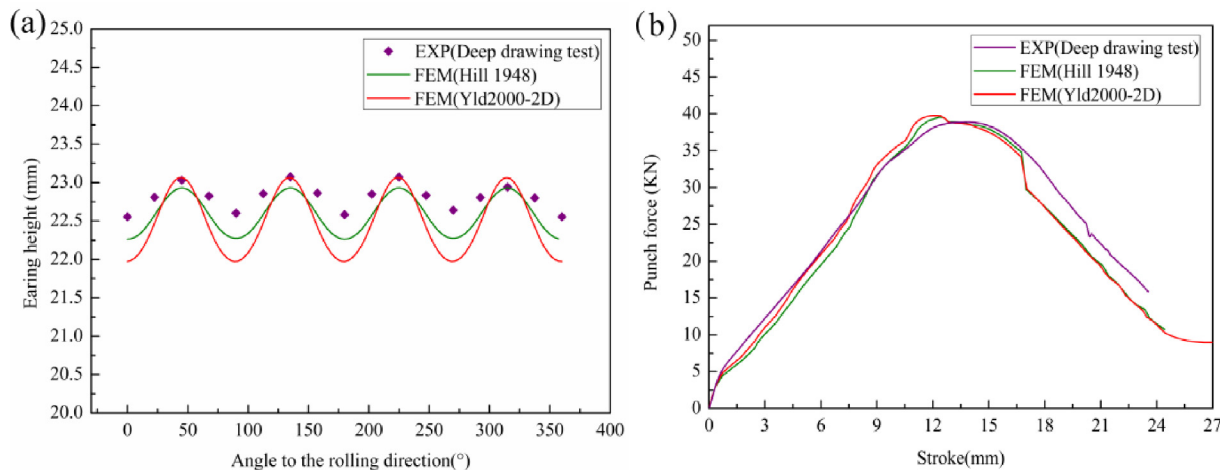


Fig. 24. Simulation earing heights and punch force in comparison with the experimental results (a) Earing heights (b) Punch force.

implemented into the FE-deep drawing model, respectively. The obtained simulation results were shown in Fig. 23. Then, the simulation earing profile was compared to the experimental one.

Fig. 24 showed the earing heights and punch force measured by experiment and predicted by the simulations based on the Yld2000-2D and Hill'48. As can be seen, the predicted earing heights and punch force were agreed with the experimental results. Compared with Hill'48 yield criterion, the earing heights prediction of the Yld2000-2D yield criterion was more consistent with the experimental tests at 50°, 130°, 230° from the rolling direction. The Yld2000-2D identified by the inverse identification method accurately predicted the highest point of upper profile of the deep drawn cup. While the earing heights predicted by Hill'48 was closer to the experimental results for the lower profiles.

By comparing the results of the simulation and experiment, it can be concluded that the conventional uniaxial tensile test with electric heating system and the inverse identification method with Potter test both accurately obtained the material property.

## Conclusions

In this paper, the plastic anisotropy behavior of 7B04 aluminum alloy at 200 °C was investigated by conventional uniaxial tensile tests with electrical heating system and Pottier test with heating rods. Several conclusions were obtained.

(1) With the designed electrical heating system, the precise heating and temperature controlling of the tensile specimens were realized. Through the temperature field measurement, effective temperature area was determined. Based on the strain measured by the DIC system within the effective temperature area, the Hill'48 yield criterion and Voce hardening of the 7B04 aluminum alloy were accurately obtained.

(2) With the heating rods and DIC system, the strain field and displacement field of the Pottier test at 200 °C were obtained. The strain field analysis showed that the Pottier specimen produced a very heterogeneous strain field during deformation. Based on the analyses of the Pottier test, an inverse identification process with the FEMU-U-F method and SIMPLEX algorithm was conducted to determine the constitutive equation parameters (Yld2000-2D with Voce hardening) of 7B04 aluminum alloy. A good match between the experiment and the simulation was obtained.

(3) A deep drawing test was conducted to verify the accuracy of the identified yield function parameters. It was shown that the determined yield function parameter sets can accurately predict the earing height and punch force, whether it was obtained by the conventional method or the inverse identification method. The uniaxial tensile test with electrical heating system and DIC system was suitable for determining the thermal-mechanical properties of the metal sheet. Furthermore, a single Potter test with FEMU-U-F method can accurately identify a advanced yield criterion

## Acknowledgements

The authors would like to acknowledge the geometry and dimensions of Pottier specimen provided by Professor Thomas Pottier (Université de Toulouse). The authors also would like to acknowledge the financial support from Natural Science Foundation of Shandong Province [grant number ZR2019MEE008], National Natural Science Foundation of China (Grant No. 51405266) and Young Scholars Program of Shandong University, Weihai (YSPSDUWH).

## Appendix A. Supplementary data

Supplementary data to this article can be found online at <https://>

doi.org/10.1016/j.rinp.2019.102655.

## References

- [1] Li Niankui, Lu Xinyu, Cui Jianzhong. Effect of processing way and aging treatment on properties and microstructures of 7B04 aluminum alloy. *Trans Nonferrous Met Soc China* 2008;18:541–7.
- [2] Lyu Fenggong, Li Yong, Huang Xia, Shi Zhusheng, Zeng Yuansong, Lin Jianguo. An investigation of creep age forming of AA7B04 stiffened plates: experiment and FE modelling. *J Manuf Process* 2019;37:232–41.
- [3] Djavanroodi F, Ebrahimi M, Janbakhsh M. A study on the stretching potential, anisotropy behavior and mechanical properties of AA7075 and Ti-6Al-4V alloys using forming limit diagram: an experimental, numerical and theoretical approaches. *Results phys* 2019;14:102496.
- [4] Pacheco M, Celentano D, García-Herrera C, Méndez J. Numerical simulation and experimental validation of a multi-step deep drawing process. *Int J Mater Form* 2017;10:15–27.
- [5] Hill R. A theory of the yielding and plastic flow of anisotropic metals. *Proc R Soc Lond Ser A: Math Phys Sci* 1948;193:281–97.
- [6] Barlat F, Brem JC, Yoon JW, Chung K, Dick RE. Plane stress yield function for aluminum alloy sheets – part 1: theory. *Int J Non Linear Mech* 2003;19:1297–319.
- [7] Bron F, Besson J. A yield function for anisotropic materials Application to aluminum alloys. *Int J Plasticity* 2004;20(4–5):937–63.
- [8] Zidane I, Guines D, Léotoing L, Ragneau Eric. Development of an in-plane biaxial test for forming limit curve (FLC) characterization of metallic sheets. *Meas Sci Technol* 2014;21(5):055701.
- [9] Prates PA, Oliveira MC, Fernandes JV. A new strategy for the simultaneous identification of constitutive laws parameters of metal sheets using a single test. *Comp Mater Sci* 2014;85(4):102–20.
- [10] Kim JH, Barlat F, Pierron F, Lee MG. Determination of anisotropic plastic constitutive parameters using the virtual fields method. *Exp Mech* 2014;54(7):1189–204.
- [11] Avril S, Bonnet M, Bretelle AS. Overview of identification methods of mechanical parameters based on full-field measurements. *Exp Mech* 2008;48(4):381–402.
- [12] Martins JMP, Andrade-Campos A, Thuillier S. Comparison of inverse identification strategies for constitutive mechanical models using full-field measurements. *Int J Mech Sci* 2018;145:330–45.
- [13] Markiewicz éric, Langrand B, Notta-Cuvier D. A review of characterisation and parameters identification of materials constitutive and damage models: from normalised direct approach to most advanced inverse problem resolution. *Int J Mech Sci* 2017;110:371–81.
- [14] Tairui Zhang, Shang Wang, Weiqiang Wang. Method to determine the optimal constitutive model from spherical indentation tests. *Results phys* 2018;8:716–27.
- [15] Jinwu Xiang, Shiwei Zhao, Daochun Li. A model updating method considering the complex mechanical environment. *Results phys* 2016;6:530–3.
- [16] Guery Adrien, Hild François, Latourte Félix, Roux Stéphane. Identification of crystal plasticity parameters using DIC measurements and weighted FEMU. *Mech Mater* 2016;100:55–71.
- [17] Souto N, Andrade-Campos A, Thuillier S. A numerical methodology to design heterogeneous mechanical tests. *Int J Mech Sci* 2016;107:264–76.
- [18] Zhang Shunying, Leotoing Lionel, Guines Dominique, Thuillier Sandrine. Potential of the cross biaxial test for anisotropy characterization based on heterogeneous strain field. *Exp Mech* 2015;55(5):817–35.
- [19] Zhu J, Huang SY, Liu W, Hu JH, Zou XF. Calibration of anisotropic yield function by introducing plane strain test instead of equi-biaxial tensile test. *Trans Nonferrous Met Soc China* 2018;28(11):2307–13.
- [20] Teaca M, Charpentier I, Martiny M, Ferron G. Identification of sheet metal plastic anisotropy using heterogeneous biaxial tensile tests. *Int J Mech Sci* 2010;52(4):572–80.
- [21] Prates PA, Oliveira MC, Fernandes JV. A new strategy for the simultaneous identification of constitutive laws parameters of metal sheets using a single test. *Comp Mater Sci* 2010;85(4):102–20.
- [22] Pottier T, Toussaint F, Vacher P. Contribution of heterogeneous strain field measurements and boundary conditions modelling in inverse identification of material parameters. *Eur J Mech A-Solids* 2011;30(3):373–82.
- [23] Rossi M, Pierron F, Štamborská M. Application of the virtual fields method to large strain anisotropic plasticity. *Int J Solids Struct* 2016;97–98:322–35.
- [24] Denys K, Coppieters S, Seefeldt M, Debruyne D. Multi-DIC setup for the identification of a 3D anisotropic yield surface of thick high strength steel using a double perforated specimen. *Mech Mater* 2016;100:96–108.
- [25] Pottier T, Vacher P, Toussaint F, Louche H. Out-of-plane testing procedure for inverse identification purpose: application in sheet metal plasticity. *Exp Mech* 2012;52(7):951–63.
- [26] Yang D, Chan YC, Wu YB, Pecht M. Electromigration and thermomigration behavior of flip chip solder joints in high current density packages. *J Mater Res* 2008;23(9):2333–9.
- [27] Cong Y. The deformation behavior, texture and microstructure evolution of aluminum alloy under electropulsing. University of Huazhong University of Science & Technology; 2015. Master thesis.
- [28] Kinsey B, Cullen G, Jordan A, Mates S. Investigation of electroplastic effect at high deformation rates for 304SS and Ti-6Al-4V. *CIRP Ann* 2013;62(1):279–82.
- [29] Zhang Xin, Li Hongwei, Yan Siliang, Zhang Ning. Experimental study and analysis on the electrically-assisted tensile behaviours of Inconel 718 alloy. *Procedia Eng* 2017;207:365–70.
- [30] Piao K, Lee KJ, Kim JH, Chung K, Balart F, Wagoner RH. A sheet tension/compression test for elevated temperature. *Int J Plasticity* 2012;38:27–46.
- [31] Information on < <http://www.esteco.com/modefrontier> > .